Geothermics 127 (2025) 103238

Contents lists available at ScienceDirect

Geothermics

journal homepage: www.elsevier.com/locate/geothermics

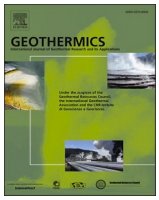

Optimizing inhibitor injection in geothermal wells with electrical submersible pump

Hakki Aydin [a,*], Seray Işık Tezel [a], Selcuk Erol [b]

[a] Zorlu Energy Group, Sarayköy, Denizli, Turkey
[b] Izmir Institude of Technology, Izmir, Turkey

ARTICLE INFO

Keywords:
Geothermal
Inhibitor dosage
ESP

ABSTRACT

Electrical submersible pump (ESP) is a reliable artificial lift method to extend productive lifespan of geothermal wells. In the geothermal industry a common practice involves installing ESPs below the well's flashing depth. This placement approach aims to mitigate the risk of mineral precipitation, which can occur when hot geothermal fluids transition to a two-phase state (liquid and vapor) as pressure decreases. Positioning the pump below the flashing depth also prevents pump's underloading and gas cavitation. The inhibitor injection line usually integrated around the ESP string and installed downstream of the ESP motor. However, this standard practice introduces a challenge regarding inhibitor performance. While this placement ensures effective distribution of inhibitors throughout the production flow, the extended travel time from the surface to the point of application at the ESP can diminish inhibitor effectiveness due to continuous exposure to high temperatures throughout the wellbore. This study proposes relocating the inhibitor injection point within the production tubing closer to the flashing depth. This reduces inhibitor travel time from 108 min to 48 min and has the potential to significantly improve inhibitor effectiveness. Consequently, the implementation of capillary tubing is anticipated to yield annual cost savings per wellbore of approximately USD 10,000, coupled with the mitigation of mineral deposits within the studied well equipped with ESP. To evaluate this approach, a wellbore simulation tool and PHREEQC were employed to dynamically model the pressure and temperature profiles alongside the geochemical evolution of the produced fluids in the wellbore. This modeling approach offers significant value by potentially enabling the optimization of inhibitor usage and reducing the length of required inhibitor injection line.

1. Introduction

The degassing of dissolved gases, such as carbon dioxide (CO_2), and geothermal water commonly changes the water chemistry, leading to mineral precipitation within the wellbore, pipelines, and separators (DiPippo 2008; DiPippo 2016; Zhang et al., 2022; Cao et al. 2024). The types of precipitated minerals may vary across different geothermal fields due to a range of geochemical composition and thermodynamic condition of aquifer fluids. The primary mechanism driving precipitation is the change in thermodynamic conditions and the degassing process, which typically occur in the wellbore during fluid flow. Changes in water composition and temperature during degassing generally lead to shifts in mineral saturation, resulting in precipitation (Tarcan, 2001). To illustrate, the precipitation of carbonate minerals such as calcite and aragonite has been reported in Gediz and Büyük Menderes grabens, Turkey (Haklıdır et al., 2019). Similarly, in the Kızıldere geothermal field in Turkey, Tarcan et al. (2016) noted that water samples exhibit an undersaturated state for calcite and aragonite, with a lower saturation index under reservoir conditions. However, these minerals become supersaturated and have a precipitation tendency in the sampling line, likely due to degassing occurring in the wellbore, pipeline, and valves. (Tonkul et al., 2022a) characterized mineral precipitation in the hypersaline geothermal system at the Tuzla geothermal power plant in northwestern Turkey. They reported galena (PbS) and calcite scaling in the wellbore Demir et al. (2014) reported the same scale composition in the Tuzla field, noting that a 7 mm thick mineral deposit formed within four months. The type of scaling may vary between the wellbore and surface infrastructure, such as injection lines and heat exchangers. Tonkul et al. (2022) investigated stibnite scaling in the preheaters of power plants at the Germencik geothermal site in western Turkey to determine the optimal reinjection temperature

* Corresponding author.
E-mail addresses: hakki.aydin@zorlu.com (H. Aydin), seray.isik@zorlu.com (S.I. Tezel), selcukerol@iyte.edu.tr (S. Erol).

https://doi.org/10.1016/j.geothermics.2024.103238
Received 23 August 2024; Received in revised form 27 November 2024; Accepted 8 December 2024
Available online 18 December 2024

Nomenclature

Q	Flowrate
U	Overall heat transfer
K	Flow parameter
T_r	Formation temperature
T	Fluid temperature
d_w	Inside well diameter
A	Internal cross sectional area of the pipe
S_g	Static gas volume fraction
v_g	Gas superficial velocity
ρ_g	Gas density
M	Total mass flow rate
Q_f	flowing quality
Q_s	static quality
S_I	static liquid volume fraction
Z	correlation variable
R_n	Reynolds number
F_r	Froude number
Y_I	flowing liquid volume fraction
W_e	Weber number
α, β,	w constants
$S.V.$	pseudo-variance

that prevents efficiency loss due to stibnite precipitation. The inhibitors are not only used for inhibiting mineral precipitation in geothermal industry but also to protect infrastructure and wellbores from corrosion. Gunnlaugsson et al. (2014) reviewed the corrosive nature of geothermal wells in Iceland, categorizing sources of corrosion as chloride, hydrogen sulfide, carbon dioxide, ammonia, oxygen, and sulfate. Similarly, van de Watering and van der Velde (2019) reported that only corrosion inhibitors are used in the geothermal sector in the Netherlands. Although this study focuses primarily on mineral deposition, the effectiveness of corrosion inhibitors is also time and temperature dependent. Therefore, understanding this relationship provides valuable insights for reducing corrosion effect.

The continuous injection of inhibitors offers a potential mitigation method for flow assurance challenges arising from mineral precipitation within geothermal wells (Mercado et al., 1989; Sugiaman et al., 2004). Inhibitors act in two different ways: On one hand they complex specific cations by forming water soluble complexes. On the other hand, they inhibit the growth of crystals by adsorption on growth active surfaces which leads thereby effectively to retardation or blocking of the growth rate (Scheiber et al. 2013). To ensure a homogeneous inhibitor mixing within the geothermal brine before it enters the two-phase zone, the inhibitor injection line is set below the flashing depth (T. Akın and Kargı, 2019). However, precise determination of the flashing depth is crucial for optimal inhibitor injection. If the injection line is lowered excessively below the flashing depth, the inhibitor chemical will be subjected to high temperatures for an extended travel time, resulting in less effectiveness. The Henry's constant approach has been effectively used to calculate the degassing pressure of a saline geothermal fluid with a specific amount of carbon dioxide at a given temperature (Cramer, 1982; Fournier, 1989). The degassing depth of a flowing well can be determined through wellbore flow simulation and by dynamically measuring the pressure and temperature profiles of the well. The depth at which the flowing pressure drops below the degassing pressure is the beginning of multi-phase flow. Numerous geothermal wellbore simulators have been developed to simulate fluid flow in geothermal production wells. These models typically use liquid hold-up correlations to model two-phase flow. Bjornsson (1987) developed a wellbore simulation model for multi-feed zone geothermal wells. Aunzo (1990) proposed a wellbore simulator called GWELL, which was based on Bjornsson's study. Upton (2000) released a wellbore simulator, SIMU2000, using a homogeneous flow model to incorporate fluid mechanics theories. Garg et al. (2003) modified the WELBOR simulation program, originally developed by Pritchett in 1985. Wasch et al. (2019) coupled a wellbore flow simulator, LedaFlow, with a geochemical modeling tool, PHREEQC, to better evaluate scaling potential. The integrated workflow was applied to a Dutch doublet and successfully mimicked the observed calcite scaling. Chauhan et al. (2021) used Euler two-phase fluid flow to simulate the degassing process, which affects calcite precipitation inside geothermal wellbores. They showed a higher likelihood of mineral deposition in sections where phase transitions occurred, leading to an increase in slip velocity. These works are recently used in artificial intelligence algorithms, typically providing input for learning and training. For example, Aydin et al. (2020) incorporated the WELBOR simulator with an artificial neural network to estimate the bottom hole flowing pressure and temperature of geothermal wells.

In the laboratory, two types of tests, namely, a static batch test and an in-line tube blocking test with different setups are used to evaluate inhibitor efficiency under high-pressure and high-temperature (HPHT) conditions (Zotzmann et al., 2018). In the static batch test, geothermal fluid and inhibitor are fully mixed, then heated and pressurized until equilibrium is reached. The extend of the scaling is quantified by monitoring a variety of fluid properties such as the electrical conductivity, pH value, concentration of ions, and amount of solid precipitation on-line during experiments, or off-line after termination of the experiments (Zotzmann et al., 2018). As an example of static batch test, Pauwells et al., (2022) examined the stability of the two different inhibitors (Diethylenetriamine Pentamethylene Phosphonic Acid and TD1100) at temperature ranging from 75 °C to 120 °C at 45 bars. They conducted the tests for seven days at 120 °C and another seven days at 75 °C to simulate the temperature drop occurring across the heat exchanger in geothermal plants. However, the autoclave experiments were performed in a batch system rather than under fluid circulation or in-line conditions. Therefore, the test may not fully mimic the heat exchanger flowing conditions. After autoclave experiments, both of the inhibitors showed inadequate stability in these conditions and lost their ability to reduce mineral scaling. Similarly, Zotzmann et al. (2018) conducted a static batch test using a stainless-steel autoclave to assess the effectiveness of inhibitors on calcite scaling under conditions up to a pressure of 150 bar and a temperature of 125–200 °C, prevailing in geothermal reservoirs. The experiments were conducted over four weeks and sampled after certain time intervals (1,2,7,14, and 28 days). They showed that the inhibitor performance decreases at HPHT compared with ambient conditions. In the in-line tube blocking test, the mixed fluid is circulated through a tube by pumping. The pressure drop across the tube, resulting from physical and chemical changes over time, is monitored to assess the inhibitor's performance (Bazin et al. 2005). The efficiency of scaling inhibitors is ranked by comparing the concentration of inhibitor required to achieve a predefined level of inhibition during fluid circulation. The lower inhibitor concentration for a scaling inhibitor, the higher its performance (Graham et al. 2006). He et al. (1996) performed dynamic flow-through inhibitor testing and developed a semi-empirical model to predict effective concentrations in oil and gas production systems. They conducted tests with polyphosphonate-based inhibitors to prevent common water scales, such as calcium carbonate, calcium sulfate, and barium sulfate, across a wide range of saturation indices, pH levels, and temperatures up to 70 °C. The study found that the inhibition efficiency increases as the solution pH increases, probably because of the advancing dissociation of the inhibitor acid. Also, the inhibition efficiency decreases as the temperature increases. Scheiber et al. (2013)

Fig. 1. Calcium carbonate scaling in a geothermal wellbore from Alaşehir field, Turkey (Tezel, 2018).

noted that the degree of efficiency of an inhibitor is impacted by several physical-chemical parameters: pH, thermal stability, adsorption affinity, and the presence and concentration of co-ions like Ca^{2+}, Mg^{2+}, Sr^{2+} or Pb^{2+} in solution, and the thermal stability of the phosphonate. A greater quantity of inhibitor is needed (He et al., 1994) with increasing temperature, and the thermally induced decomposition of phosphonates must also be taken into account (Scheiber et al. 2013).

In field applications, the inhibitor dosing system is attached to the ESP string and is positioned below the ESP's motor. In this practice, the inhibitor dosing concentration is typically adjusted to determine the optimal concentration for scale inhibition (Wylde and Fell, 2008a). However, the thermal exposure time of the inhibiting chemical is also a critical parameter that affects the dosing concentration. Most studies in the literature focus on the thermal stability tests of scale inhibitors and do not address the modeling of dynamic pressure, temperature, and geochemical simulations along the wellbore. This study begins with a wellbore flow simulation to determine the thermodynamic properties of geothermal fluid along the wellbore, including the flashing depth. Subsequently, the geochemical profile of the fluid is obtained using PHREEQC to identify potential mineral precipitations. Unlike standard industry practices, the inhibitor dosage tubing is configured differently to reduce the inhibitor's travel time, thereby minimizing exposure to high temperatures.

In this study, a liquid blended product based on organic phosphate and dispersants was used to investigate thermal stability and the effect of travel time, specifically determining the duration the inhibitor is exposed to high temperatures. The dosage of the inhibitor depends on various factors, including conductivity, hardness, well depth, travel time, and temperatures of inhibitor exposure. Thermal exposure tests in autoclaves were conducted using a stirrer and autoclaves at a pH of 8.2, with a temperature range of 180–220 °C, 35 bar pressure, and a duration of 3 h. The results showed no performance reduction for calcium carbonate inhibition. However, in the beaker test, the metal-silicate inhibition performance decreased by >10 %, and the sulfide inhibition performance dropped by about 5 % at 180 °C after one hour. The performance reduction was found to be linear over time. Both the literature studies mentioned above, and the scale inhibitor used in this study demonstrate that the efficiency of inhibitors in geothermal systems is highly dependent on their thermal stability, as well as other critical parameters previously discussed. Therefore, reducing thermal exposure time will decrease the dosage of inhibitor needed for scale inhibition. Considering other parameters remain the same, decreasing high-temperature exposure time may reduce the required inhibitor dosage.

As an illustration of wellbore diameter reduction, Tezel (2018) presented a scaling issue in Alaşehir geothermal field, mainly calcium carbonate precipitation in the production wells (Fig. 1). Similarly,

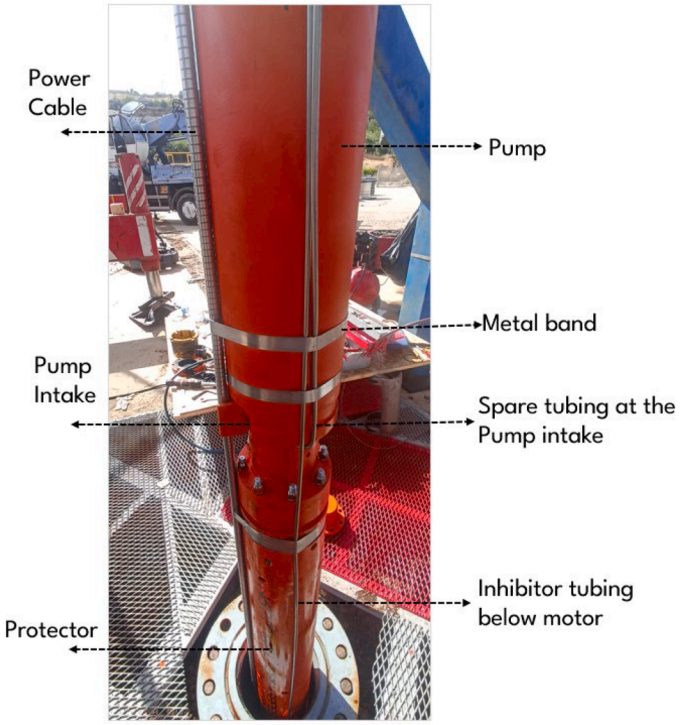

Fig. 2. A view from ESP installation in Alaşehir field, showing inhibitor injection lines and ESP parts.

Haklıdır and Balaban (2019) characterized mineral precipitation of geothermal wells in western Anatolia. Their findings indicated that calcite deposition was the dominant form of mineral scaling observed within production wells. Phosphonate polymer-based inhibitors were suggested to address clogging issues in these wells.

The flashing depth is influenced by a range of flow and well parameters, including reservoir temperature, pressure, non-condensable gas (NCG) content, and production flow rate. Strong connectivity between injection and production wells generally ensures effective pressure support but it may reduce both temperature and NCG production, resulting in a shallower flashing depth. Consequently, it is essential to conduct periodic dynamic pressure and temperature (PT) surveys to update the conditions of dynamic wells. To illustrate, Akin et al. 2020 reported a substantial NCG decline of Alaşehir field, in Turkey due to high connectivity between injection and production wells. Additionally, Aydin and Akin (2021) observed a premature temperature decline in the same field, likely attributable to cold reinjection brine. Effective pressure support, coupled with reduced NCG and production temperature, can collectively shift the flashing depth shallower points in the wellbore. Therefore, to maintain optimal inhibitor delivery, it becomes essential to regularly monitor and adjust the depth of the inhibitor injection line based on these dynamic well conditions.

Electrical submersible pumps (ESPs) are effectively utilized in geothermal wells with low reservoir pressure and gas content (Aydin and Merey, 2021). The recent studies are focused on ESP design and performance. Yang et al. (2021) analyzed pressure pulsation in multi-stage ESPs, which causes noise and vibration. They found that pressure interference between the impeller and diffuser is the main cause of pressure pulsation. Similarly, Han et al. (2023) investigated the effects of tip clearance on the energy performance of multi-stage ESPs. They predicted flow loss in the ESPs, leading to an optimized design of the ESPs.

In the industry-standard practice of inhibitor injection for ESP applications, the inhibitor injection line is attached to the ESP string and positioned below the ESP motor (Fig. 2 and Fig. 3). The current practice may lead to inhibitor deposition in the pump. J.J. Wylde and Fell (2008)

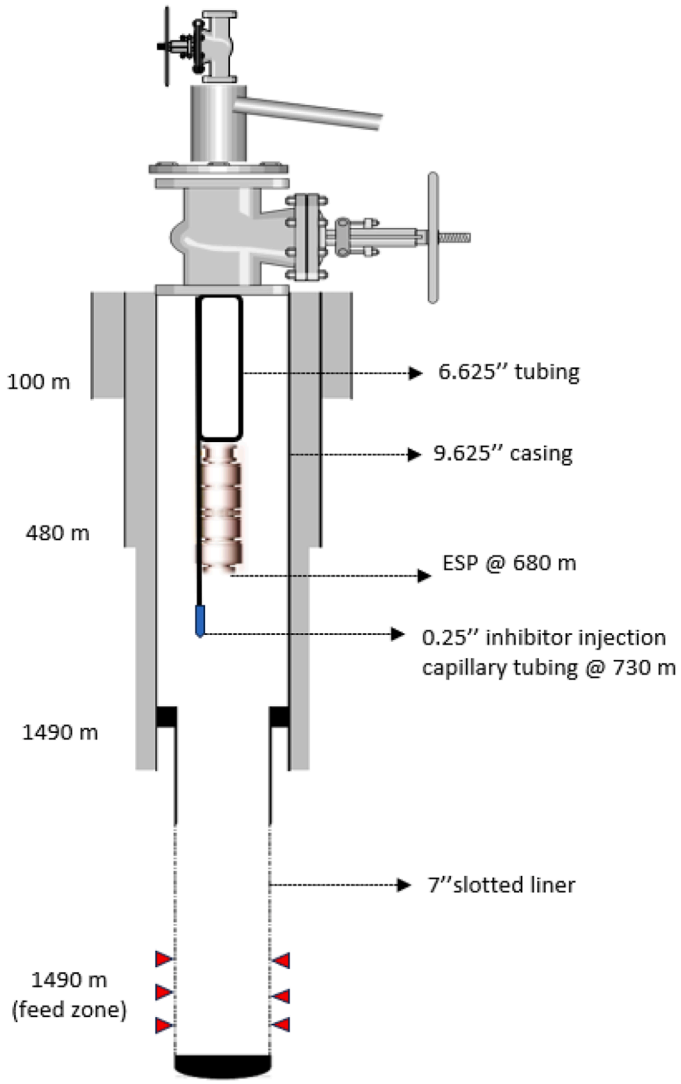

Fig. 3. Industrial practice for inhibitor dosage in geothermal wells with ESP.

reported inhibitor deposition on the pump resulting in ESP failure. However, since the ESP is set below the flashing depth, the geothermal fluid is pressurized within the pump, initiating the flashing process in the production tubing at a shallower depth. Therefore, the standard practice of inhibitor injection is inefficient due to the prolonged travel time of the inhibitor, which results in extended exposure to high temperatures. Therefore, a higher inhibitor concentration is required for inhibiting mineral precipitation. Besides, shortening the length of the tubing has led to a higher inhibitor concentration at the surface, resulting in more effective inhibition.

To predict wellbore flow and scaling conditions, different wellbore simulators were coupled mostly with geochemical modeling tool PHREEQC. For instance, Abouie et al. (2017) developed a wellbore simulator (UTWELL) coupled with geochemical modeling tool IPHREEQC to calculate multiphase flow and deposition of solid particles in the wellbore. Bozou et al., (2015) utilized PHAST wellbore model tool to inspect corrosion effects and barite scaling in geothermal wellbores using PHREEQC. On the other hand, Cen and Jiang (2018) developed a novel tool to couple multiphase flow and geochemical modeling as a wellbore simulator.

This study was motivated by observations in the Alaşehir geothermal field, where a significant decrease in reservoir temperature and NCG content and pressure maintenance through reinjection support resulted in a substantial shift in the flashing depth to the shallower depths. Flashing depths previously were ranging from 400 to 700 m, shifted to a shallower depth between 50 and 300 m for various wells' characteristics. Consequently, the depth of inhibitor injection capillary tubing was revised. It was found that this revision improved the effectiveness of the inhibitor chemical, allowing for a reduction in the dosage concentration from 2.5 ppm to 1 ppm. These observations suggested the possibility of achieving the same effect by adjusting the inhibitor dosing depth in ESP applications.

Based on observations of successful inhibitor injection in artesian wells, this study aimed to investigate and mitigate inhibitor-associated mineralization within the pump and production casing (6 5/8″) of a geothermal well equipped with an ESP. Mineral deposits observed in the ESP string were hypothesized to result from prolonged inhibitor residence time, leading to degradation (burning) and subsequent reactions with other elements to form mineral deposits. In geothermal power plants in Western Anatolia, common scale control methods involve chemical inhibitors, including phosphate salts, phosphonate salts, and polymer-formulated inhibitors (Haklıdır and Balaban, 2019). We propose relocating the inhibitor capillary within the 6 5/8-inch production tubing closer to the flashing depth. This reduces inhibitor travel time and has the potential to significantly improve inhibitor effectiveness. To evaluate this approach, a wellbore simulation tool (WELBOR) and a geochemical modeling tool (PHREEQC) were employed to dynamically model the pressure and temperature profiles alongside the geochemical evolution of the produced fluids throughout the wellbore. This modeling approach offers significant value by potentially enabling the optimization of inhibitor usage and reducing the length of required inhibitor capillary tubing.

2. Materials and methods

Following verification with dynamic pressure-temperature (P&T) surveys from well X-3, the WELBOR software was employed to simulate the P&T profile of well X-10 equipped with ESP. Additionally, PHREEQC software was utilized to perform a geochemical evaluation of the geothermal fluid along the wellbore of well X-10.

The WELBOR code is designed to model the steady-state flow of water, steam, and carbon dioxide within a borehole. The working flow diagram of the WELBOR is illustrated in Fig. 4. To utilize this code, users must provide specific input parameters related to the well's geometry, including the internal diameter and the angle of deviation from the vertical along the length of the borehole (Aydin et al. 2020). The WELBOR model employs a steady-state solver that utilizes empirical correlations to address the complex dynamics of two-phase flow in geothermal wellbores. Specifically, it applies the Dukler I correlation (Dukler et al., 1964) to calculate frictional pressure drop as part of the pressure and temperature profile calculations along the wellbore. This solver iteratively adjusts parameters to align with observed downhole and wellhead measurements, rather than functioning as a fully transient or time-dependent solver. The WELBOR model does not explicitly use a drift flux model. Instead, it relies on empirical correlations, including the Dukler I correlation, to account for slip between the liquid and gas phases in two-phase flow. While drift flux models typically describe velocity differences between phases, WELBOR indirectly addresses phase slip by adjusting liquid hold-up and friction factors. It incorporates a modified version of the Hughmark correlation (Hughmark, 1962) to adjust liquid hold-up along the wellbore, allowing for relative motion between phases without directly implementing a drift flux approach. Furthermore, the WELBOR model does not directly utilize a mixture model in its calculations. Instead, it approximates two-phase flow of steam and water by applying separate empirical correlations for liquid hold-up and friction factor, which capture the behavior of each phase individually. This method, combined with the Dukler I correlation, enables WELBOR to calculate the overall pressure and temperature profiles without directly solving for mixture equations. It manages each phase through empirical adjustments, differing from the combined

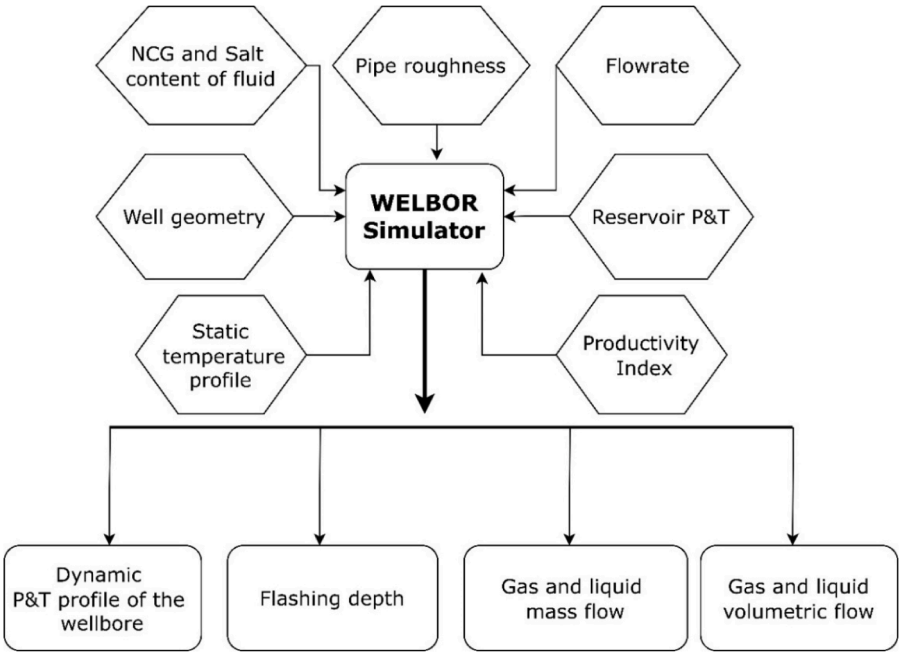

Fig. 4. Working flow diagram of WELBOR (Created from Garg and Pritchett, 2001; Garg et al. 2004).

phase equations typically used in traditional mixture model approaches.

The users need to specify a stable formation temperature profile with depth and an "effective thermal conductivity" to represent the conductive heat transfer between the wellbore fluid and the surrounding geological formation (Garg and Pritchett, 2001). Key parameters such as static reservoir pressure, temperature, and productivity index at the flowing feed point must also be defined (Fig. 4).

The WELBOR code discretizes the length of the wellbore into smaller intervals, from the bottom of the well to the wellhead for fluid flow calculations. During fluid flow, heat transfer and momentum loss are calculated within these intervals. Temperature reduction in the wellbore fluid is attributed to both adiabatic processes and conductive heat transfer to the surrounding formations.

During fluid flow in the wellbore, at a given wellhead flowing temperature, pressure, and flow rate, phase transition begins at a depth known as the flashing point. Steam and carbon dioxide gas (CO_2(g)) start to separate from the geothermal brine. The dissociated CO_2(g) and steam create partial pressure during the two-phase flow. As a result, the wellhead flowing pressure and temperature are influenced by momentum loss, heat loss, and the flashing process along the length of the wellbore. A variety of flow patterns, such as slug, churn, and annular flow, may occur as fluid ascends in the wellbore, determined by the relative amounts of gas and liquid. Pritchett (1985) and Garg et al. (2003) employed modified Hughmark liquid holdup (Hughmark, 1962) and Dukler I friction (Dukler et al., 1964) correlations to simulate two-phase flow in geothermal wells. The WELBOR uses Eq. (1) to calculate heat transfer between the fluid and the surrounding formations, assuming an outward-directed heat flux. The heat transfer coefficient is approximated using Eq. 2. Garg et al. (2004) reported a typical value for liquid flow in geothermal wellboreas 4 W/m/ °C. The liquid holdup correlation establishes a relationship between flowing and static gas quality (through Eqs. (3)-(6)).

$$Q = U\ (T - T_r \tag{1}$$

where T represents local temperature of the fluid in the wellbore, T_r is the undisturbed formation temperature, and U is an overall heat transfer coefficient (W/m^2/ °C).

$$U = \frac{0.6K}{d_w}\ (T - T_r \tag{2}$$

Where K is the effective thermal conductivity of the formation and d_w is the inside well diameter.

$$Q_f = \frac{AS_g p_g v_g}{M} \tag{3}$$

$$Q_f = \frac{Q_s}{[1 - Q_s]K + Q_s\left[1 - \frac{p_l(1-K)}{p_g}\right]} \tag{4}$$

$$Q_s = \frac{S_g p_g}{p_m} \tag{5}$$

$$p_m = S_l p_l + S_g p_g \tag{6}$$

Where, A is the cross-sectional area of the pipe, M is the total rate, Q_s is the static quality, Q_f is the flowing quality, p_m is mixture density, p_g is gas density, K is a flow parameter, v_g and v_l represents superficial gas and liquid velocity, S_l and S_g are static liquid and gas volume fraction. For homogeneous flow (no slip) the static quality is equal to the flowing quality and flow parameter is equal to unity. Due to buoyancy, gas phase is expected to rise more rapidly than liquid, which implies Eq.7.

$$Q_f \geq Q_s \ and\ S_g \leq K \leq 1 \tag{7}$$

$$K = K(Z(R_n, F_r, Y_I, W_e,\ S_I)) \tag{8}$$

where, R_n, F_r, Y_I, W_e and S_I are the variables used by (Hughmark, 1962). To find a correlation for K, Garg et al. (2004) used a single variable Z:

$$Z = K\left(Z\left((R_n)^{\alpha}(F_r)^{\beta}(Y_I)^{y}(S_I)^{w}\right)\right) \tag{9}$$

where α, β, y and w are undetermined exponents, which can be estimated by minimizing the variance between the calculated and measured values for K. Garg et al. (2004) introduced a non-parametric measure of variation:

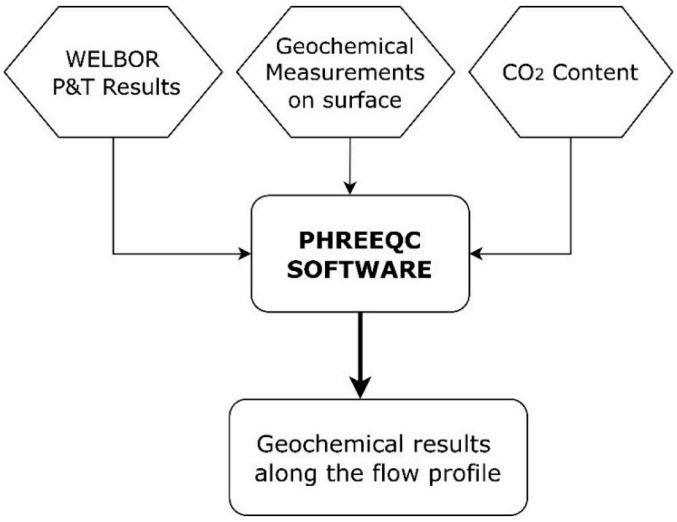

Fig. 5. Working flow diagram of the simulation with PHREEQC.

$$S.V. = \sum_{i=1}^{n-1} (K_{i+1} - K_i)^2 \tag{10}$$

where K_i denotes the value of K corresponding to Z_i, n is the number of points in the dataset, and Z_n is the largest value of Z. The exponents are obtained by minimizing the pseudo-variance ($S.V.$). To verify the holdup correlation an improved version of WELBOR code was created by Garg et al. (2004).

In this study, PHREEQC version 3, a robust geochemical modeling software, is utilized to simulate geochemical processes occurring within the wellbore during flow (Parkhurst and Appelo, 2013). The working diagram of the PHREEQC is illustrated in Fig. 5. PHREEQC offers a comprehensive range of capabilities, including the determination of mineral saturation indices and speciation, the modeling of mineral and gas equilibria, advective transport calculations, inverse modeling for parameter estimation, the simulation of surface complexation reactions, and the incorporation of ion exchange reactions (Parkhust, 2005). PHREEQC utilizes the Peng-Robinson equation of state and fugacity concept (Peng and Robinson, 1976) to model CO_2 solubility in the aqueous phase. Furthermore, various thermodynamic databases, such as PITZER, Palandri, LLNL, and the PHREEQC database itself, can be

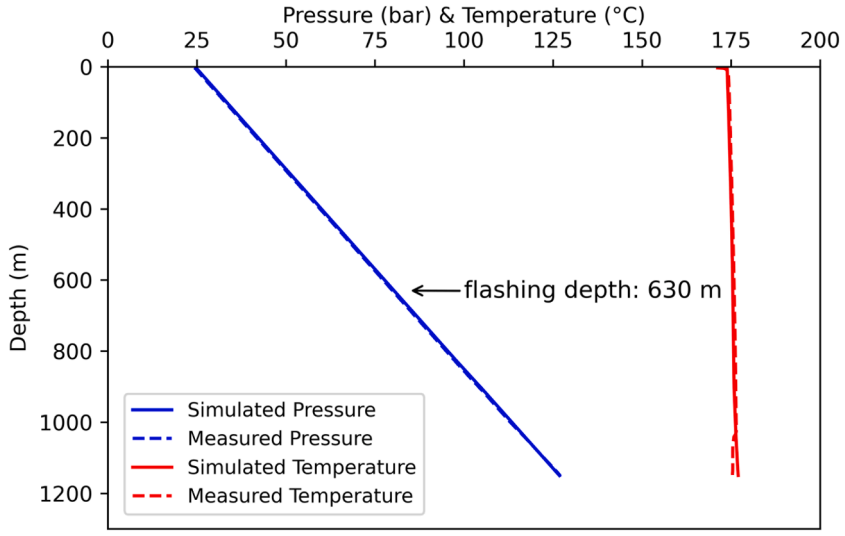

Fig. 6. Dynamic PT survey and Wellbore simulation of well X-1 for January 2016.

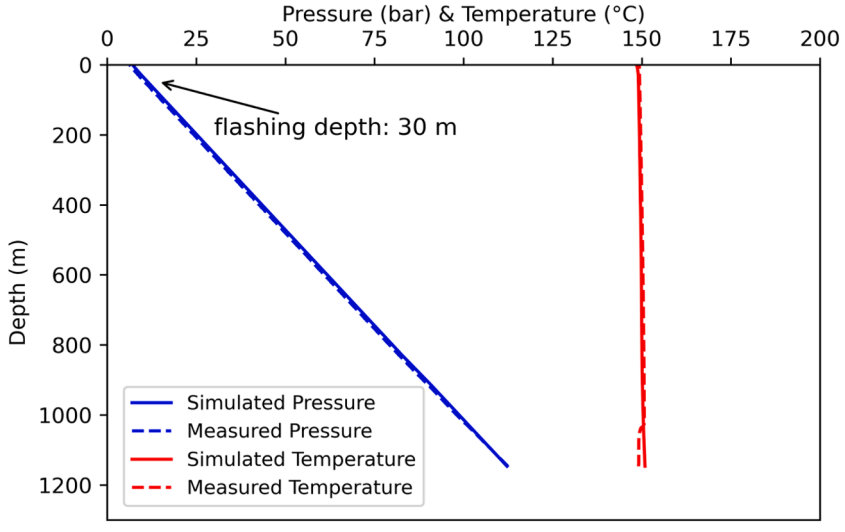

Fig. 7. Dynamic PT survey and Wellbore simulation of well X-1 for January 2023.

Table 1
Geochemical measurements for capillary tubing at depths 450 m and 100 m at well X-1.

Capillary Injection tubing at 450 m depth				Capillary Injection tubing at 100 m depth			
T (°C	27	Br^{-}(mg/l)	1.1562	T (°C	22.2	Br^{-}(mg/l)	1.200
pH	6.546	NO_3^{-}(mg/l)	0.0814	pH	6.538	NO_3^{-}(mg/l)	0.333
EC (µS/cm)	2170	SO_4^{-2} (mg/l)	30.281	EC (µS/cm)	2380	SO_4^{-2} (mg/l)	17.803
F^{-}(mg/l)	9.879	PO_4^{-3} (mg/l)	0.7993	F^{-}(mg/l)	9.111	PO_4^{-3} (mg/l)	1.370
Cl^{-}(mg/l)	270.52	Li^{+}(mg/l)	3.478	Cl^{-}(mg/l)	280.507	Li^{+}(mg/l)	3.325
K^{+}(mg/l)	39.047	Na^{+}(mg/l)	523.556	K^{+}(mg/l)	36.380	Na^{+}(mg/l)	507.35
SiO_2 (mg/l)	256	NH_4^{+}(mg/l)	18.113	SiO_2 (mg/l)	253	NH_4^{+}(mg/l)	18.488
Ca^{+2} (mg/l)	9	Mg^{+2} (mg/l)	0.45	Ca^{+2} (mg/l)	9.1	Mg^{+2}(mg/l)	0.33

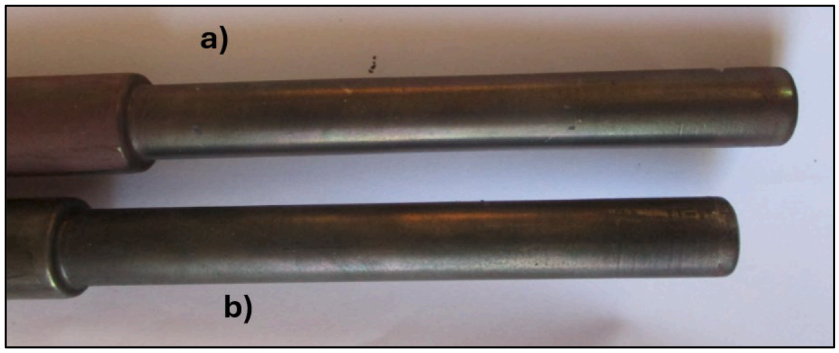

Fig. 8. Coupon view for a) Capillary tubing at 450 m b) at 100 m depth.

integrated with PHREEQC to simulate fluid geochemistry under diverse thermodynamic conditions (Hörbrand et al. 2018). Recent geochemical studies investigating geothermal wells in Western Anatolia with similar water compositions (Akın and Kargı, 2019b; Erol et al., 2023a; Aydin and Akin, 2023) demonstrated that the best matches were obtained with the LLNL database comparison to field measurements and experimental evaluations. Therefore, we have used LLNL as reference database in this study.

3. Results and discussion

This study was motivated by the observation of a significant enhancement in inhibitor effectiveness following an adjustment of the injection depth based on updated wellbore dynamics. As aforementioned above, the Alaşehir field experienced a substantial decline in NCG content and reservoir temperature, which has been attributed to re-injection well connectivity. Aydin and Akin (2020) corroborated this finding through the implementation of a comprehensive tracer test within the Alaşehir field. Besides, reservoir temperature was reduced from 176 °C to 150 °C as shown in Fig. 6 and Fig. 7. Consequently, the flashing depth of the well-X3 exhibited a significant reduction, shifting from a depth of 630-meter (Fig. 6) to 30-meter (Fig. 7) within a production timeframe of seven years.

Before changing the setting depth, reducing the inhibitor dosing depth led to a decline in the total hardness of the fluid sampled at the wellhead, indicating the presence of mineral scale. Following an updated P&T survey in well X-1, the depth of the capillary tubing was adjusted from 450-meter to 100-meter in 2023. This adjustment resulted in a reduction of inhibitor travel time from 97 min to 21 min. Consequently, due to increased inhibitor effectiveness, the dosage concentration was lowered from 2.5 ppm to 1 ppm. Table 1 presents geochemical data collected before and after this capillary tubing depth optimization in 2023. Geochemical measurements (Table 1) suggests a slight decrease in SiO_2 and Mg^{+2} indicating magnesium-silicate precipitation; however, the observed changes are negligible, and no precipitation was evident on coupons (Fig. 8) retrieved from the production line at the wellhead.

Geochemical modeling of well X-1 was conducted using PHREEQC

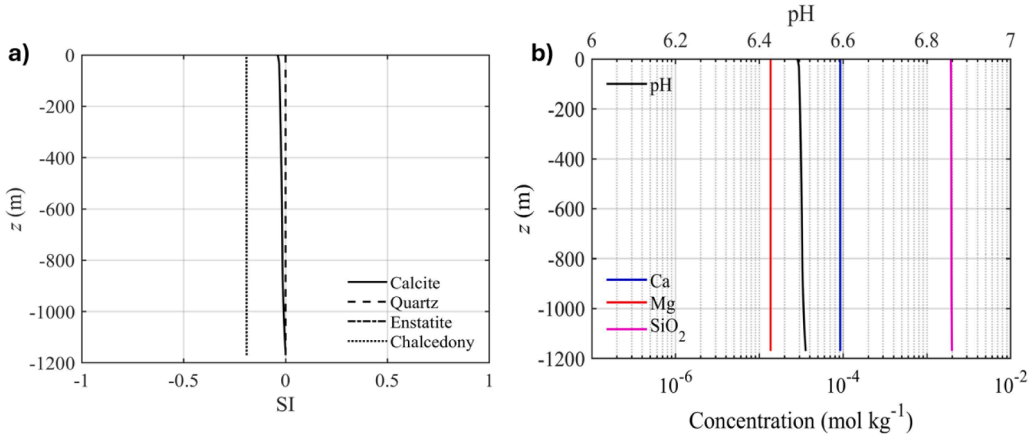

Fig. 9. Geochemical modeling of well X-1: a) Saturation index of minerals and b) concentration of elements along the flow profile.

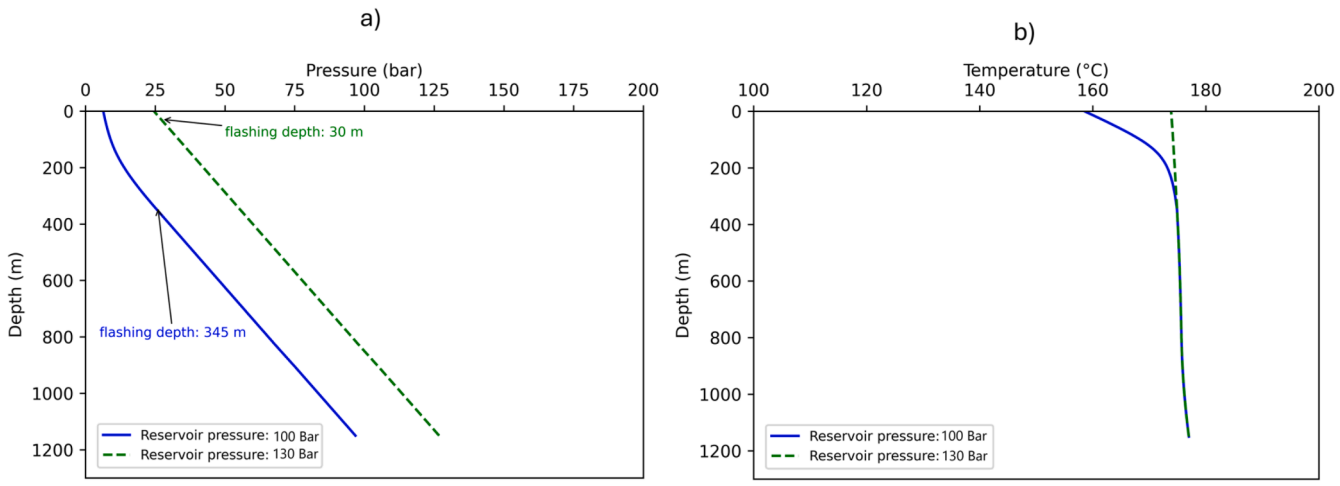

Fig. 10. Sensitivity analysis with a reservoir pressure of 100 bar and 130 bar a) Pressure profile, b) Temperature profile.

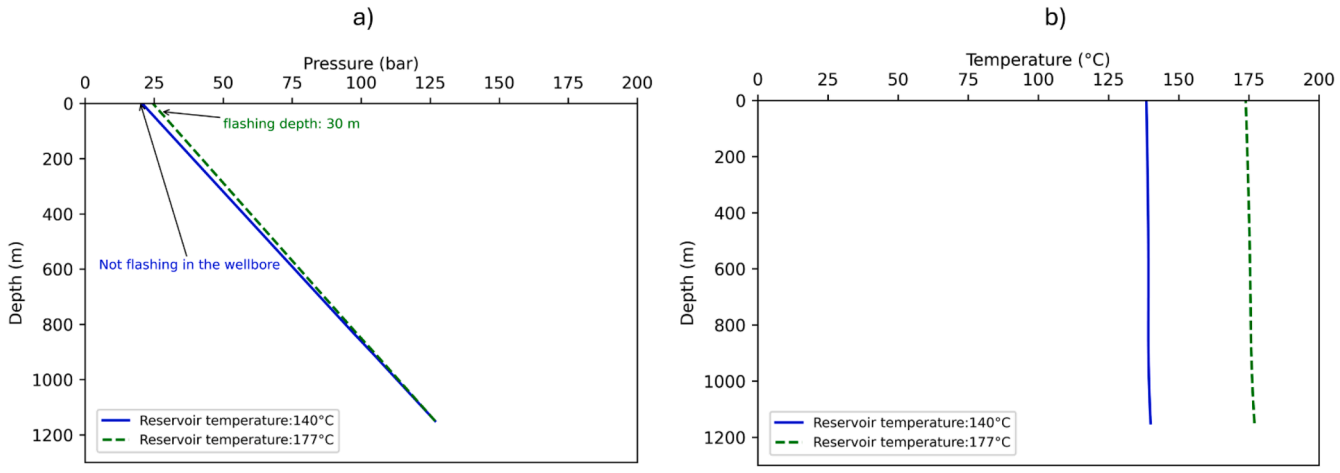

Fig. 11. Sensitivity analysis with a reservoir temperature of 177 °C and 140 °C a) Pressure profile, b)Temperature profile.

Fig. 12. Precipitation materials collected from inside of 6 5/8-inch casing.

(Fig. 9). The calculated mineral saturation indices (Fig. 9a) exhibited good agreement with the results obtained from coupon analyses and geochemical measurements (Table 1). Furthermore, no significant changes were observed in the concentrations of calcite, magnesium, silicate elements, or wellbore fluid pH along the flow profile (Fig. 9b). This suggests that minerals such as calcite, quartz, chalcedony, and enstatite are currently undergoing dissolution, with no evidence of precipitation.

A sensitivity analysis was conducted in WELBOR to understand how changes in reservoir pressure and temperature conditions affect the wellbore pressure and temperature profiles, with a specific focus on the flashing depth. When reservoir pressure was decreased from 130 bar to 100 bar, the flashing depth dropped from 30 m to 345 m from the wellhead (Fig. 10a). Additionally, the decline in wellhead flowing temperature became more pronounced due to the phase transition, falling below 160 °C, compared to 174 °C at a reservoir pressure of 130 bar (Fig. 10b). A sensitivity analysis was also conducted on the reservoir temperature to demonstrate its effects on changes in flashing depth. It was found that as the reservoir temperature decreased from 177 °C to 140 °C, the wellhead flowing pressure was reduced by 5 bar However,

Table 2
XRF results of the deposit material accumulated on internal surface of casing.

Si / %	Mg / %	Fe / %	Ca / %	P / %	Ba / %	Sr / %	Mn / %
13.1	5.23	4.21	2.14	0.83	0.14	0.12	0.094
Ti / %	S / %	Sb / %	K / %	As / %	Hg / %	Cu / %	Ag / %
0.077	0.063	0.06	0.051	0.021	0.012	0.012	0.008
W / %	Ni / %	Pb / %	Zn / %	Se / %	Rb / %	Bi / %	Y / %
0.008	0.008	0.007	0.007	0.005	0.003	0.003	0.002
Tl / %	Al / %	Nd / %	Pr / %	Ce / %	La / %	Co / %	Cs / %
0.002	<0.12	<0.065	<0.050	<0.043	<0.038	<0.029	<0.019

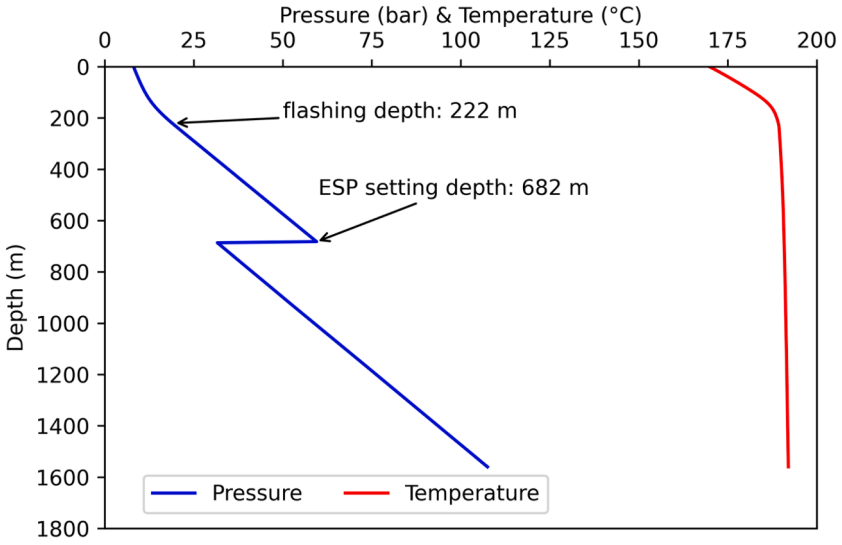

Fig. 13. Simulated P&T profile of well X-10 with ESP application.

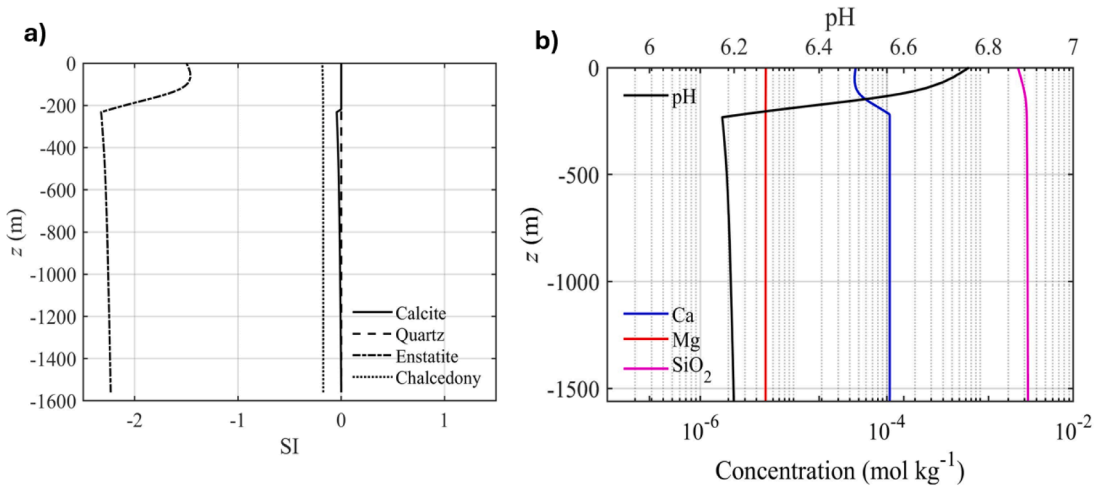

Fig. 14. Geochemical modeling of well X-10 with ESP: a) Saturation index of minerals and b) concentration of elements along the flow profile.

no flashing was observed in the wellbore due to the lower saturation pressure associated with the lower temperature (Fig. 11).

Fig. 12 illustrates the accumulation of precipitated material on the internal casing surface of ESP string. Table 2 presents the results of X-ray Fluorescence (XRF) analysis performed on the mineral deposits. The analysis suggests the presence of magnesium-silicate and calcium-phosphate phases. This result was also reported by Nowak (2003), who noted that a high concentration of co-ions can trigger the precipitation of metal-phosphonates. The observed presence of iron may be attributed to contamination from the carbon-steel casing during sample collection from the casing surface.

To investigate the mineral deposition problem within well X-10, a simulation of its dynamic pressure-temperature (P&T) profile was conducted with WELBOR (Fig. 13). The simulation revealed that the pressure at the pump intake is already higher than the flashing pressure. The increased pressure within the pump leads to a calculated flashing depth for well X-10 of approximately 222 m.

Geochemical modeling of well X-10 was performed using PHREEQC software (Fig. 14). The calculated mineral saturation indices (Fig. 14a) indicate a trend of precipitation for calcite and magnesium silicate (enstatite) from a depth of approximately 222 m towards the wellhead. This finding is further corroborated by the observed decrease in the

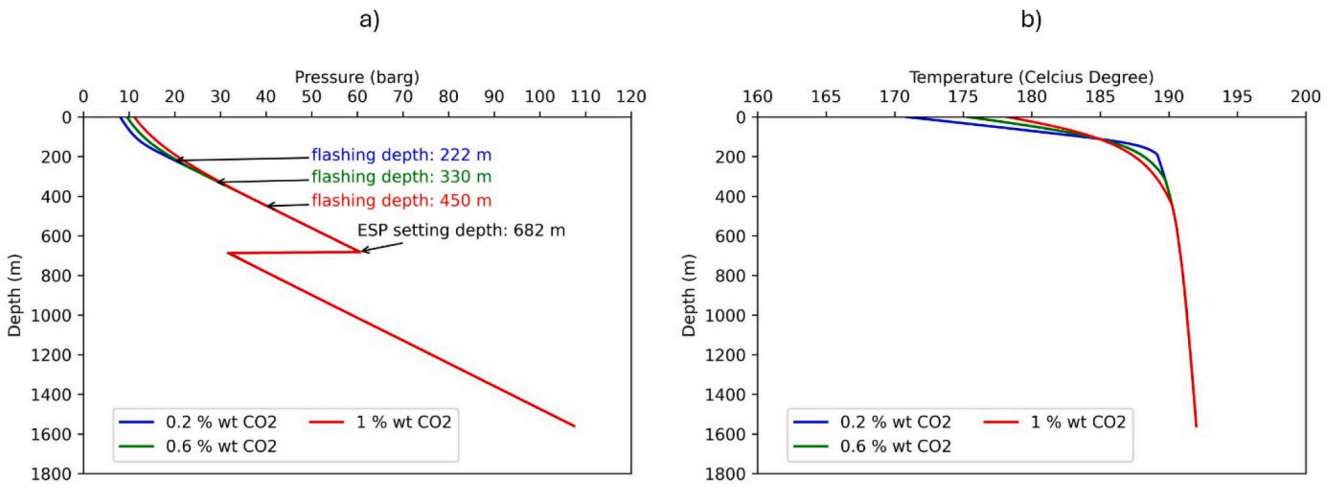

Fig. 15. Simulated pressure a) and temperature b) profile for different CO_2 contents.

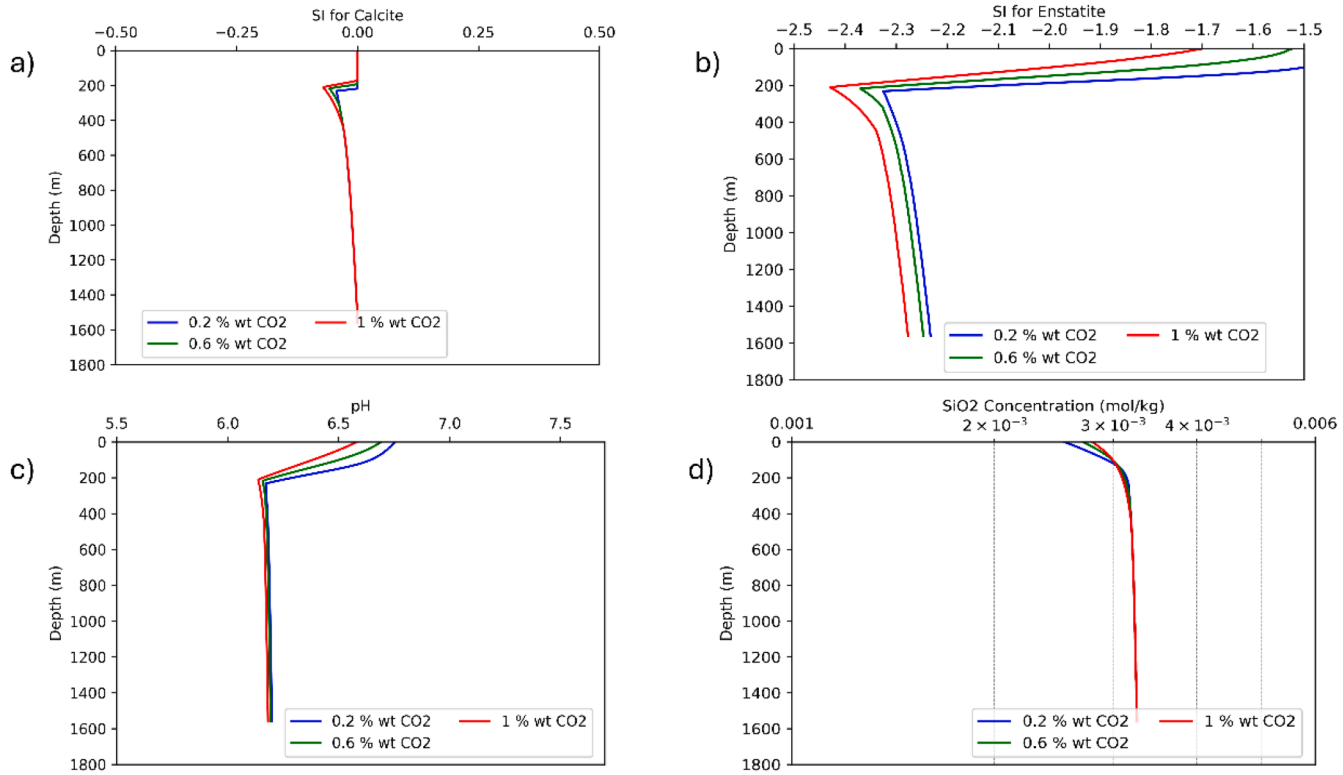

Fig. 16. Geochemical modeling of well X-10 with ESP: a) Saturation index of minerals and b) concentration of elements along the flow profile.

concentration of calcium and silica elements within the brine (Fig. 14b). The increasing pH profile of the geothermal fluid (Fig. 14b) is also consistent with a flashing process occurring around 222 m. This rise in pH can be attributed to the dissociation of CO_2 gas from the geothermal brine.

To increase the reliability of the proposed model, a sensitivity analysis was performed in WELBOR using parameters such as productivity index, flow rate, casing roughness, salt content, reservoir pressure, and reservoir temperature, all kept constant except for the CO_2 content. The P&T profile of the wellbore was simulated for different CO_2 weight contents of 0.2 %, 0.6 %, and 1 % (Fig. 15). It was found that as the CO_2 content increased, the degassing depth occurred at a greater depth (Fig. 15a). The temperature profile of the cases aligns with the pressure profile due to thermodynamic equilibrium. The temperature profile decreases as water transitions from liquid to gas (steam), and it begins to decrease at greater depths with higher CO_2 content due to degassing (Fig. 15b).

Using the P&T profiles obtained from WELBOR with different cases of CO_2 content, the PHREEQC model was employed to show the effects of varying conditions on the geochemical profile along the wellbore. The calculated mineral saturation indices (Fig. 16a) indicate a trend of calcite precipitation beginning at the depths where degassing occurs for CO_2 concentrations of 0.2 %, 0.6 %, and 1 %. To prevent mineral precipitation related scaling issues, inhibitor injection line should be set below degassing depth for each case. A similar behavior was observed for Enstatite (Fig. 16b), however SI is negative along the wellbore. The variation of the SI exists along the wellbore profile because a higher CO_2 content results in a lower pH value (Fig. 16c). Silica precipitation begins

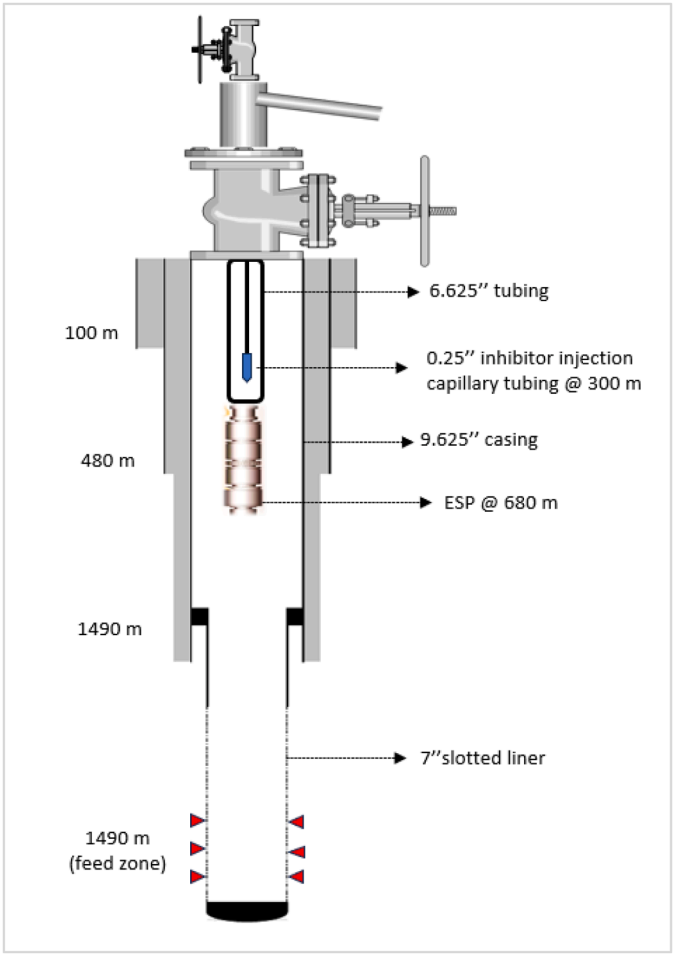

Fig. 17. Proposed inhibitor dosage configuration for well X-10 with ESP.

at the degassing depth and was found to be higher in the case with lower CO_2 content (Fig. 16d). Silica dissolution increases at pH values above 9 and below 5 (Utami et al. 2014; Bush et al. 2018). Therefore, higher CO_2 content is favorable for SiO_2 dissolution in brine with a pH lower than 7.

To address the observed mineral deposition within well X-10 and achieve inhibitor effectiveness comparable to that observed in artesian well X-1, we propose the deployment of capillary tubing within the production casing of the ESP string at a depth of approximately 300 m (Fig. 17). This approach aims to reduce the inhibitor residence time from 108 min to 48 min, thereby enhancing inhibitor effectiveness and mitigating mineral precipitation. This leads to a reduction in inhibitor dosage from 3 ppm to 1 ppm. Shortening the length of the tubing has led to a higher inhibitor concentration at the surface, resulting in more effective inhibition. Additionally, the pH value shows an increasing trend due to CO_2 degassing, which enhances the progressive dissociation of the phosphonate inhibitor, thereby increasing its effectiveness. A similar result was reported by (He et al., 1996). Therefore, it can be inferred that the effectiveness of the inhibitor increases from the depth at which flashing occurs to the surface. Scheiber et al. (2013) found similar results from efficiency tests of a phosphonate-based inhibitor in laboratory and on-site studies in Soultz-sous-Forêts, France. They noted that phosphonates are very effective at very low concentrations. This type of threshold inhibition is related to adsorption of phosphonates or their dissociated compounds on growth-active surfaces (Weijnen and Van Rosmalen, 1986; He et al., 1996). As a consequence of these adsorption processes the crystal morphology shifts from typically idiomorphic crystals to smoothed and rounded surfaces (Black et al., 1991).

The inhibitor dosage was reduced from 3 ppm to 1 ppm and the required length of capillary tubing is expected to be diminished by approximately 400 m. Consequently, the implementation of capillary tubing is anticipated to yield annual cost savings of approximately USD 10,000, coupled with the mitigation of mineral deposits within the well X-10.

A potential limitation of the proposed design is that the current 1.5-inch diameter sinker bar may cause a reduction in the flow cross-sectional area within the production casing. To mitigate this concern, we recommend using a 1-inch diameter sinker bar, thereby ensuring an unrestricted flow cross-section. An additional potential risk associated with the proposed design is the possibility of ESP malfunction in the event of sinker bar failure or capillary tubing loss.

4. Conclusion

This investigation aims to enhance inhibitor effectiveness within geothermal wells. The motivation of this research stemmed from a prior observation of significantly improved inhibitor performance following an adjustment of the injection depth based on updated wellbore dynamics. Drawing upon this principle, namely inhibitor injection closer to the flashing depth, the present study proposes the relocation of capillary tubing within the production casing of the ESP string. Although the current study focuses on a geothermal well with an ESP, the methodology can be applied to any type of well. The following key conclusions can be drawn from this work:

- The industry-standard practice of inhibitor injection for ESP applications, the inhibitor injection line is attached to the ESP string and positioned below the ESP motor leads to mineral deposition in the pump and production casing.
- The integration of wellbore flow simulation using WELBOR and geochemical modeling with PHREEQC proved to be an effective approach for determining the precise location of the flashing point for optimal inhibitor dosage
- Magnesium-silicate and calcium carbonate were identified as the dominant mineral deposits within geothermal wells located in Alaşehir field, in Western Anatolia.
- Relocating the capillary tubing within the production casing is projected to achieve a reduction in inhibitor travel time from 108 min to 48 min. This intervention is anticipated to yield annual cost savings of approximately USD 10,000 while concurrently mitigating mineral deposition within well X-10.
- To ensure an unrestricted flow cross-sectional area within the production casing, the proposed design is recommended to utilize a 1-inch diameter sinker bar.

CRediT authorship contribution statement

Hakki Aydin: Writing – review & editing, Writing – original draft, Visualization, Validation, Supervision, Software, Resources, Methodology, Investigation, Formal analysis, Conceptualization. **Seray Işık Tezel:** Resources. **Selcuk Erol:** Writing – review & editing, Writing – original draft, Visualization, Validation, Supervision, Software, Resources, Formal analysis, Data curation, Conceptualization.

Declaration of competing interest

The authors declare that they have no known competing financial interests or personal relationships that could have appeared to influence the work reported in this paper.

The authors declare that they have no known competing financial interests or personal relationships that could have appeared to influence the work reported in this paper.

Acknowledgment

The authors thank Sabodh Garg for providing WELBOR program for this study.

Data availability

The data that has been used is confidential.

References

Abouie, Ali, Korrani, Aboulghasem, Kazemi, Shirdel, Mahdy, Kamy, Sepehrnoori, 2017. Comprehensive modeling of scale deposition by use of a coupled geochemical and compositional wellbore simulator. SPE J 22 (2017), 1225–1241.

Akin, S., Aydin, H., Akin, T., 2020. CO_2 decline in Alaşehir (Turkey) geothermal reservoir. In: In Proceedings World Geothermal Congress (p. 1).

Akın, T., Kargı, H., 2019. Modeling the geochemical evolution of fluids in geothermal wells and its implication for sustainable energy production. Geothermics 77, 115–129.

Aunzo, Z.P., 1990. GWELL: A Multi-Component Multi-Feedzone Geothermal Wellbore Simulator. University of California at Berkeley, Berkeley, CA, USA. M.S. Thesis.

Aydin, H., Akin, S., 2021. Estimation of upcoming problems in Alaşehir geothermal field using a numerical reservoir model. Arab. J. Geosci. 14, 1–20.

Aydin, H., Akin, S., 2023. CO2 Dissolution in the reservoir brine: an experimental and simulation-based approach. Geothermics 113, 102774.

Aydin, H., Merey, S., 2021. Design of electrical submersible pump system in geothermal wells: a case study from West Anatolia, Turkey. Energy 230, 120891.

Aydin, H., Akin, S., Senturk, E., 2020. A proxy model for determining reservoir pressure and temperature for geothermal wells. Geothermics 88, 101916.

Bazin, B., Kohler, N., Zaitoun, A., 2005. Some insights into the tube blocking test method to evaluate the efciency of mineral scale inhibitors. In: SPE annual technical conference, 96560. SPE, Dallas.

Black, S., Bromley, L., Cottier, D., Davey, R., Dobbs, B., Rout, J., 1991. Interactions at the organic/inorganic interface: binding motifs for phosphonates at the surface of barite crystals. J. Chem. Soc. Farad. Trans., 87 (1991), 3409–3414.

Bjornsson, G., 1987. A multi-Feedzone geothermal wellbore simulator. Earth Sciences Division. Report LBL-23546.

Bush, J.A., Vanneste, J., Gustafson, E.M., Waechter, C.A., Jassby, D., Turchi, C.S., Cath, T.Y., 2018. Prevention and management of silica scaling in membrane distillation using pH adjustment. J. Memb. Sci. 554, 366–377.

Cao, B., Ma, Y., Liu, M., Li, S., Tian, H., Feng, G., 2024. Predictions of locations of flash point and calcite scaling of geothermal fluids in wellbore by chemical and thermodynamic simulations. Geothermics 121, 103057.

Cen, J.; Jiang, F. A practical field test and simulation procedure for prediction of scaling in geothermal wells containing Noncondensable gases. *Processes* 2022, 10, 2018. https://doi.org/10.3390/pr10102018.

Chauhan, V., Saevarsdottir, G., Tesfahunegn, Y.A., Asbjornsson, E., Gudjonsdottir, M., 2021. Computational study of two-phase flashing flow in a calcite scaled geothermal wellbore. Geothermics 97, 102239.

Cramer, S.D., 1982. The solubility of methane, carbon dioxide and oxygen in brines from 0 to 300°C. Report of Investigations 8706.

Demir, M.M., Baba, A., Atilla, V., İnanlı, M., 2014. Types of the scaling in hyper saline geothermal system in northwest Turkey. Geothermics 50, 1–9.

DiPippo, R., 2008. Geothermal powerplants. Principles, Applications, Case Studies, and Environmental Impact, 2nded. Elsevier, Butterworth-Heinemann.

DiPippo, D., 2016. Geothermal Power Plants: principles. Applications, Case Studies and Environmental Impact, 4th Edition. Butterworth-Heinemann, MA, US. https://doi.org/10.1016/B978-0-08-100879-9.00025-2.

Erol, S., Akın, T., Akın, S., 2023a. Update for reactive transport modeling of the Kızıldere geothermal field to reduce uncertainties in the early inspections. Turkish J. Earth Sci. 32 (4), 541–554. https://doi.org/10.55730/1300-0985.1860.

Fournier, R.O., 1989. Lectures on geochemical interpretation of hydrothermal waters. In: Proc. of the UNU Geothermal Training Programme, p. 72. Reykjavík, Iceland, Report 10.

Garg, S.K., Pritchett, J.W., Alexander, J.H., 2003. Development of new holdup correlation for geothermal wells: a preliminary report. Trans. Geotherml. Res. Council 27, 801–806.

Garg, S.K., Pritchett, J.W., 2001. Development of new geothermal wellbore holdup correlations using flowing well data. Sci. Appl. Int. Corp. San Diego, California. Report No. SAIC-01/1061.

Graham, A.L., Boak, L.S., Neville, A., Sorbie, K.S., 2006. How Minimum inhibitor concentration and sub-MIC concentrations afect bulk precipitation and surface scaling rates. SPE 93311. SPE Prod Oper 21, 19–25, 2006.

Gunnlaugsson, E., Ármannsson, H., Thorhallsson, S., Steingrímsson, B., 2014. Problems in Geothermal Operation–Scaling and Corrosion. Geothermal Training Program, United Nations University, pp. 1–18.

Haklıdır, F.S.T., Balaban, T.Ö., 2019. A review of mineral precipitation and effective scale inhibition methods at geothermal power plants in West Anatolia (Turkey). Geothermics 80, 103–118.

Han, Y., Bai, L., Du, D., Shi, W., Zhou, L., 2023. Effects of tip clearance on energy performance of three-stage electrical submersible pump. Geoenergy Sci. Eng. 226, 211696.

He, S., Kan, A., Tomson, M., 1996. Mathematical inhibitor model for barium sulfate scale control. Langmuir 12, 1901–1905.

Hörbrand, T., Baumann, T., Moog, H.C., 2018. Validation of hydrogeochemical databases for problems in deep geothermal energy. Geotherm. Energy 6 (1), 20.

Zhang, Liang, Geng, Songhe, Chao, Jiahao, Yang, Linchao, Zhao, Zhen, 2022. Guangxiong Qin. Shaoran Ren.

Mercado, S., Bermejo, F., Hurtado, R., Terrazas, B., Hernandez, L., 1989. Scale incidence on production pipes of Cerro Prieto geothermal wells. Geothermics 18 (1–2), 225–232.

Parkhust, D.L., 2005. PHREEQC, Modeling of Geochemical Reactions, Calculation of pH, Redox Potential. PHREEQCI, Windows Interactive Version of PHREEQC. PHRQCGRF, Code to Create Graphs from the Data Generated By PHREEQC. U.S. Geological Survey.

Pritchett, J.W., 1985. WELBOR: a computer program for calculating low in a producing geothermal well. Report No. SSS-R-85-7283. S-Cubed La Jolla, California (Now Science Applications International Corporation. San Diego, California.

Scheiber, J., Seibt, A., Birner, J., Genter, A., Moeckes, W., 2013. Application of a scaling inhibitor system at the geothermal power plant in Soultz-sous-Forêts: laboratory and on-site studies. In: Proceedings of the European Geothermal Congress, pp. 3–7.

Sugiaman, F., Sunio, E., Molling, P., Stimac, J., 2004. Geochemical response to production of the Tiwi geothermal field, Philippines. Geothermics 33 (1–2), 57–86.

Tarcan, G., 2001. Aquifer chemistry and mineral saturation in selected high temperature geothermal areas. Geothermal Training programme, Orkustofnun, Grensásvegur 9. United Nations University, Reykjavík, Iceland.

Tarcan, G., Özen, T., Gemici, Ü., Çolak, M., Karamanderesi, İ.H., 2016. Geochemical assessment of mineral scaling in Kızıldere geothermal field, Turkey. Environ. Earth Sci. 75, 1–19.

Tezel, S., 2018. Hydrogeology and Geochemistry of the Alaşehir Piyadeler Geothermal Field. Manisa. MSc Thesis of Department of Geological Engineering in 9 Eylül University, İzmir, Turkey.

Tonkul, S., Baba, A., Demir, M.M., Regenspurg, S., 2022a. Investigation of Stibnite (Antimony) Scale in Germencik Geothermal Site, Büyük Menderes Graben, Western Turkey. EGU General Assembly 2022, Vienna, Austria. https://doi.org/10.5194/egusphere-egu22-9238, 23–27 May 2022, EGU22-9238.

Tonkul, S., Baba, A., Demir, M.M., Regenspurg, S., Kieling, K., 2022b. 3D modelling and characterization of scale types in hyper saline geothermal system in Tuzla geothermal power plant, NW Turkey. In: Procedings of the European Geothermal Congress.

Upton, S.P., 2000. The wellbore simulator SIMU2000. In: Proceedings World Geothermal Congress. Tohoku, Japan.

Utami, W.S., Herdianita, N.R., Atmaja, R.W., 2014. The effect of temperature and pH on the formation of silica scaling of Dieng geothermal field, Central Java, Indonesia. In: Proceedings, Thirty-Ninth Workshop on Geothermal Reservoir Engineering. Stanford University, California.

Wylde, J.J., Fell, D.A., 2008a. Scale inhibitor solutions for high temperature ESP lifted wells in California: a case history of failure followed by success. In: SPE International Oilfield Scale Conference and Exhibition. SPE-113826.

van de Watering, F., van der Velde, R., 2019. Environmental impact of inhibitors applied in the geothermal sector in the Netherlands. In: Paper presented at the European Geothermal Congress 2019, Den Haag, The Netherlands.

Wasch, L., Shoeibi-Omrani, P., Twerda, A., 2019. Integrated scale management for geothermal. In: Proceedings of the European Geothermal Congress (Vol. 6).

Weijnen, M., Van Rosmalen, G, 1986. Adsorption of phosphonates on gypsum Crystalls. J Cryst Growth 79 (1986), 157–168.

Wylde, J.J., Fell, D.A., 2008, May. Scale inhibitor solutions for high temperature ESP lifted Wells in California: a case history of failure followed by success. In: SPE International Oilfield Scale Conference and Exhibition (pp. SPE-113826). SPE.

Yang, Y., Zhou, L., Shi, W., He, Z., Han, Y., Xiao, Y., 2021. Interstage difference of pressure pulsation in a three-stage electrical submersible pump. J. Petrol. Sci. Eng. 196, 107653.

Zotzmann, J., Vetter, A., Regenspurg, S., 2018. Evaluating efficiency and stability of calcite scaling inhibitors at high pressure and high temperature in laboratory scale. Geotherm Energy 6, 18. https://doi.org/10.1186/s40517-018-0105-4.